Conformations of Gly_nH^+ and Ala_nH^+ Peptides in the Gas Phase

Robert R. Hudgins, Yi Mao, Mark A. Ratner, and Martin F. Jarrold
Department of Chemistry, Northwestern University, Evanston, Illinois 60208 USA

ABSTRACT High-resolution ion mobility measurements and molecular dynamics simulations have been used to probe the conformations of protonated polyglycine and polyalanine (Gly_nH^+ and Ala_nH^+, $n = 3$–20) in the gas phase. The measured collision integrals for both the polyglycine and the polyalanine peptides are consistent with a self-solvated globule conformation, where the peptide chain wraps around and solvates the charge located on the terminal amine. The conformations of the small peptides are governed entirely by self-solvation, whereas the larger ones have additional backbone hydrogen bonds. Helical conformations, which are stable for neutral Ala_n peptides, were not observed in the experiments. Molecular dynamics simulations for Ala_nH^+ peptides suggest that the charge destabilizes the helix, although several of the low energy conformations found in the simulations for the larger Ala_nH^+ peptides have small helical regions.

INTRODUCTION

The α-helix is among the most common short-range structural motifs in proteins (Chou and Fasman, 1974). It has been suggested that α-helix forming propensities are intrinsic to particular amino acids (Chakrabartty and Baldwin, 1995; Marqusee et al., 1989; O'Neil and DeGrado, 1990) and that solvent effects are often helix-destabilizing (DiCapua et al., 1991). However, the extent to which the α-helix-forming propensities reflect the intrinsic properties of the residues, regardless of the environment that they are in, has not been resolved. The intramolecular interactions that are intrinsic to the residues can be distinguished from those that are solvent-driven by structural analysis of polypeptides in the gas phase. Here we describe a study of the conformations of protonated polyglycine and polyalanine (Gly_nH^+ and Ala_nH^+, $n = 3$–20) in the gas phase. We chose polyglycine and polyalanine for these studies because, in addition to being the simplest naturally occurring amino acids, the helix forming propensities of these two residues in solution are radically different. Glycine has one of the lowest helix forming propensities, whereas alanine has been found to have the highest, by several experimental methods (Chakrabartty and Baldwin, 1995).

A variety of techniques have recently been used to examine the gas-phase conformations of proteins and peptides (Clemmer et al., 1995; Collings and Douglas, 1996; Gross et al., 1996; Kaltashov and Fenselau, 1997; Klassen et al., 1995; Suckau et al., 1993; Sullivan et al., 1996; Valentine et al., 1997; Wyttenbach et al., 1996). In this study, we have used high-resolution ion mobility measurements (Dugourd et al., 1997; Hudgins et al., 1997). The mobility of a gas-phase ion is a measure of how rapidly it travels through an inert buffer gas driven by a weak electric field. This approach can resolve different gas-phase conformations and provide accurate values for their collision integrals (collision cross-sections). Structural information is deduced by comparing the measured collision integrals with collision integrals calculated for model conformations such as those derived from molecular dynamics simulations.

There have only been a few structural studies of polyamino acids in the gas phase. Cassady and collaborators (Zhang et al., 1993) have measured gas-phase basicities and performed quantum chemical calculations for small polyglycines. Kebarle and collaborators (Klassen et al., 1995) have determined the onset of self-solvation-induced cyclization by equilibrium hydration measurements for Gly_nH^+, $n \leq 4$. Bowers and collaborators (Wyttenbach et al., 1998) have performed ion mobility measurements for Gly_nH^+, $n = 1$–6, which show that these species have a self-solvated globule conformation dominated by the interaction of the charged N terminus with several Lewis base groups from the peptide backbone.

Ion mobility measurements

A schematic diagram of the high resolution ion mobility apparatus (Dugourd et al., 1997; Hudgins et al., 1997) is shown in Fig. 1. The apparatus consists of an electrospray source coupled to a 63-cm long drift tube, followed by a quadrupole mass spectrometer and ion detector. Mobilities are measured by determining the amount of time it takes for a packet of ions to travel through the drift tube. The drift tube contains 46 drift guard rings that are coupled to a voltage divider to provide a uniform electric field along its length. A drift field of approximately 160 V/cm^{-1} and a helium buffer gas pressure of approximately 500 Torr were used. Note that unlike the injected ion drift tube apparatus used in many of our previous studies (Clemmer et al., 1995) the ions are not collisionally heated as they enter the drift tube region of this apparatus.

The polypeptide solutions were electrosprayed in air with 4–5 kV between the needle and the entrance plate of the drift tube apparatus. Ions are carried into the drift tube apparatus through a 0.125-mm diameter aperture in the

Received for publication 17 July 1998 and in final form 16 December 1998.
Address reprint requests to Dr. Martin Jarrold, Department of Chemistry, Northwestern University, 2145 Sheridan Road, Evanston, IL 60208. Tel.: 847-491-7553; Fax: 847-491-7713; E-mail: mfj@nwu.edu

0006-3495/99/03/1591/07 $2.00

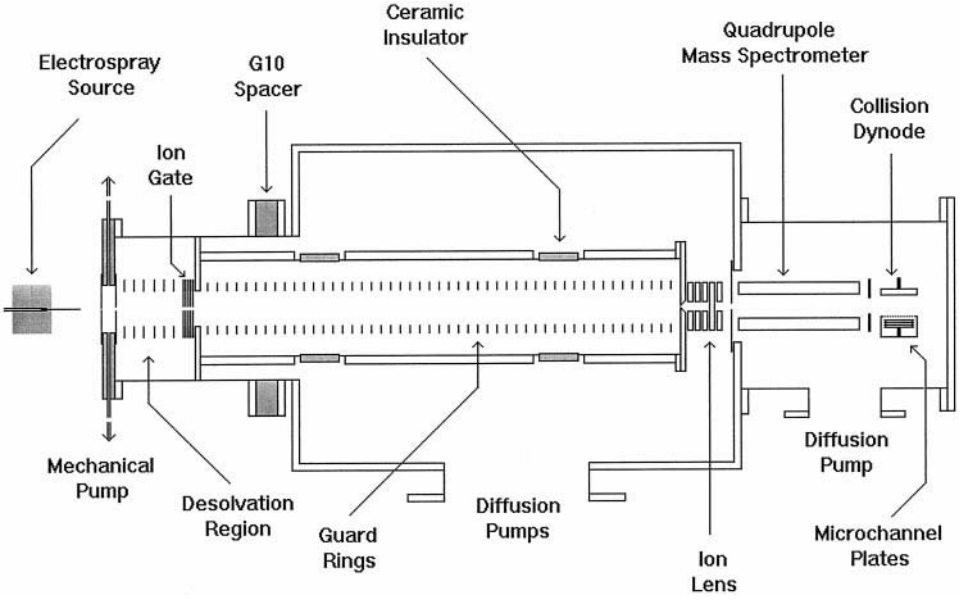

FIGURE 1 Schematic diagram of the high-resolution ion mobility apparatus.

entrance plate. They enter a small volume that is separated from the rest of the apparatus by a 6.4-mm diameter aperture. A liquid-nitrogen-trapped mechanical pump pumps away a substantial fraction of the air and solvent that enters through the entrance aperture along with the helium buffer gas that is drawn into this region. The ions are carried to the ion gate by a 400-V/cm electric field. The ion gate consists of a cylindrical channel 0.5 cm in diameter and 2.5 cm long. Helium buffer gas flow (approximately 1800 sccm) along this channel prevents air and solvent molecules from passing into the drift tube region. The ion gate is made out of a stack of ten plates and a uniform electric field of 400 V/cm carries the ions through against the buffer gas flow. The plate nearest to the entrance of the drift tube is divided into two. The voltages on these two half plates are rapidly switched to allow a short packet of ions to enter the drift tube. A pulse width of 750 μs was used. At the end of the drift tube, some of the ions exit through a 0.125-mm diameter aperture. These ions are focussed into a quadrupole mass spectrometer, and after being mass analyzed, they are detected by an off-axis collision dynode and dual microchannel plates. Drift time distributions are recorded with a multichannel scaler that is synchronized with the switching of the voltages on the half plates in the ion gate.

Molecular dynamics simulations

Molecular dynamics simulations were performed using the CHARMM force field (Brooks et al., 1983) with the 21.3-parameter set. The bond lengths were constrained by SHAKE (Van Gunsteren and Berendsen, 1977), and CH, CH_2, and CH_3 units were treated as united atoms (Weiner et al., 1984). Electrospray ionization of polyglycine and polyalanine produces $(M + H)^+$ ions that result from the addition of a single proton. The protonation site is assumed to be the nitrogen at the N terminus, and the charge is delocalized over the neighboring atoms. The N terminus has the highest pK_a in solution and gas-phase proton affinity measurements and ab-initio calculations for small homopolymers of glycine and alanine are consistent with protonation at the terminal amine (Zhang et al., 1993). The simulations were performed with a time step of 1 fs. A dielectric constant of 1 was used (this essentially ignores electronic polarization and is probably appropriate for small, isolated peptides). Most of the simulations were run at 300 K. At this temperature, equilibration to a stable conformation was generally achieved within 20–100 ps, though sometimes metastable conformations persisted for $>$1000 ps before collapsing to a lower energy structure.

A variety of starting conformations were used: a fully extended, all-trans conformation; an α-helix; and conformations in which the protonated N-terminus was pointed toward different backbone carbonyl groups of an extended random conformation. Generally, several stable conformations were found for each peptide.

To search for lower energy conformations, some simulations were performed at 1000 K for 15 ps and then quenched to 300 K. Simulations were also performed at 500 and 700 K.

Collision integral calculations

In order to compare the molecular dynamics simulations with the experimental results it is necessary to calculate collision integrals for the conformations in the molecular dynamics simulations. In this study, the cross-sections were calculated by the trajectory method recently described by Mesleh et al. (1996). The He-polypeptide potential consisted of a sum of two body Lennard-Jones interactions and ion-induced dipole interactions. For the ion-induced dipole interactions, the charge distribution from the CHARMM 21.3 parameter set was used. The Lennard-Jones parameters

used were $\epsilon = 1.34$ meV and $r_o = 3.042$ Å for C, N, and O atoms with He, and $\epsilon = 0.65$ meV and $r_o = 2.38$ Å for H with He. Because the interatomic distances fluctuate somewhat during a molecular dynamics simulation, 50 snapshots were taken over a period of 60 ps after the energy and conformation had equilibrated. Collision integrals were then calculated for the 50 snapshots and averaged.

Electrospray mass spectra

Initial experiments were performed with commercial polyglycine and poly-L-alanine from Sigma (St. Louis, MO). Commercial polyglycine and poly-L-alanine contain a broad distribution of oligomer sizes, and the mass spectra showed evidence of extensive multimer formation. Clemmer and collaborators have recently reported studies of multimer formation in the electrospray ionization of peptides (Counterman et al., 1998). To simplify the mass spectra, polyglycine and poly-L-alanine were synthesized in a narrower size distribution using continuous-flow Fmoc chemistry on a Pioneer Peptide Synthesizer (Perseptive Biosystems, Framingham, MA). HBTU or HATU (Perseptive Biosystems) and DIPEA were used as coupling reagents, and a 95/5 trifluoroacetic acid/water mixture was used for cleavage following a CH_2Cl_2 wash. The cleavage product was diluted with water or ethyl ether and lyophilized. The solid product was washed with water and DMF, and then redissolved in a solvent for electrospraying. $(Gly)_n$ and $(Ala)_n$, $n = 3$–6, were purchased from Sigma.

Electrospray mass spectra recorded for unpurified Gly_{20} and Ala_{20} are shown in Fig. 2. Poly-L-alanine is insoluble in aqueous and organic solvents (Katchalski and Sela, 1958) and very acidic organic acids are typically used to dissolve it. A variety of solvents were used (formic acid (FA), 90% trifluoroethanol/FA, 90% acetonitrile/FA, 90% acetic acid/trifluoroacetic acid (TFA), and pure TFA for poly-L-alanine and FA and TFA for polyglycine) and gave similar results. The mass spectra in Fig. 2 were obtained using a formic acid solution. In addition to Gly_{20} and Ala_{20} substantial amounts of smaller peptides are present. The coupling efficiency in the solid-phase peptide synthesis of hydrophobic homopolymers is relatively low. In addition, the highly acidic solvents required to dissolve polyalanine slowly hydrolyzes it to produce smaller peptides.

Drift time distributions

Drift time distributions measured for Gly_nH^+ and Ala_nH^+, $n = 16$–20, are shown in Fig. 3. The distributions are dominated by a single sharp peak. The dashed line in the figure shows the peak expected for a single rigid structure traveling through the drift tube. The position of this peak is arbitrary; the width of the peak is determined by the length of the injected ion pulse and the effects of diffusion as the ions travel through the drift tube. For the smaller peptides the measured peaks have widths close to that expected for a single structure, although for the larger peptides the measured peaks become slightly broader. For $Ala_{20}H^+$, which has by far the broadest peak, the measured width is approximately 1.5 times wider than expected for a single structure.

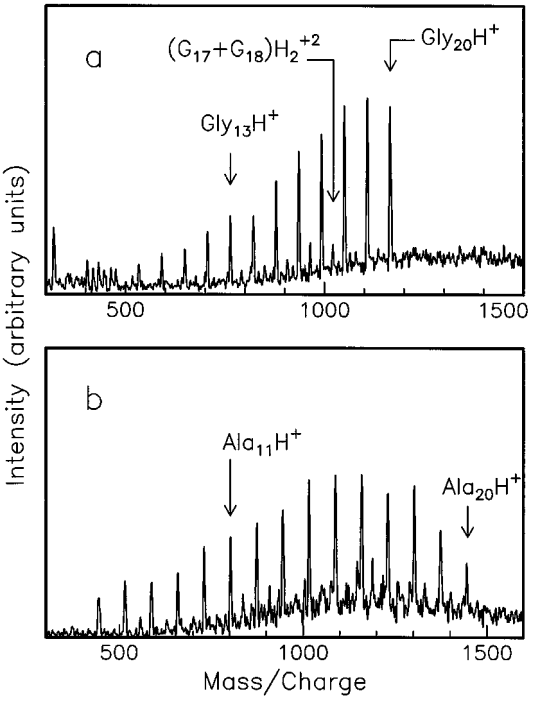

FIGURE 2 Electrospray mass spectra of unpurified Gly_{20} and Ala_{20} in formic acid at 300 K.

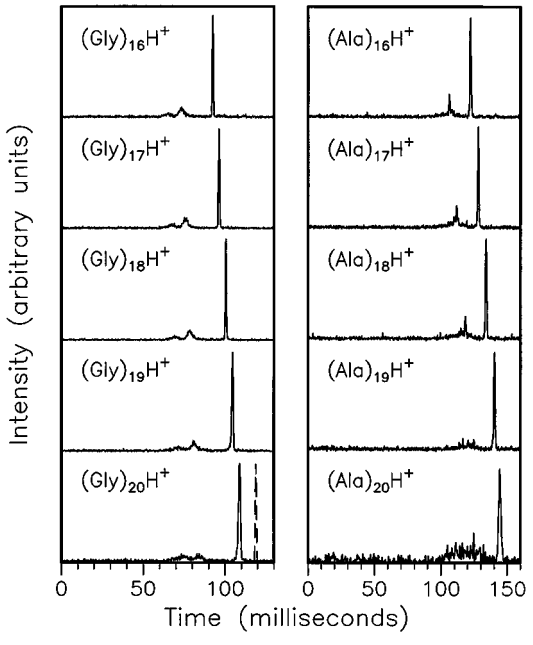

FIGURE 3 Drift time distributions measured for Gly_nH^+ and Ala_nH^+, $n = 16$–20. The dashed line shows the peak width (the position is arbitrary) expected for a single rigid structure traveling through the drift tube.

As can be seen from Fig. 3, in addition to the sharp peak there are several broader features at slightly shorter times. These features are attributed to multiply charged multimers. In the mass spectra shown in Fig. 2 there are small peaks between the main peaks. For example, the peak labeled $(G_{17} + G_{18})H_2^{2+}$ falls between the peaks assigned to $Gly_{17}H^+$ and $Gly_{18}H^+$. In addition to $(Gly_{17} + Gly_{18})H_2^{2+}$, other $(Gly_j + Gly_k)H_2^{2+}$ dimers with j, k given by 16,19 and 15,20 can contribute to this peak. In the same way, $(Gly_j + Gly_k)H_2^{2+}$ dimers with j, k given by 17,19 and 16,20 can contribute to the peak assigned to $Gly_{18}H^+$. Drift time distributions measured with the mass spectrometer set to the odd dimer peaks such as $(Gly_{17} + Gly_{18})H_2^{2+}$ are similar to the features present at short times in the drift time distributions in Fig. 3 so these features are assigned to multimers.

The measured drift times are converted into average collision integrals (collision cross-sections) using (Mason and McDaniel, 1988)

$$\Omega_{avg}^{(1,1)} = \frac{(18\pi)^{1/2}}{16}\left[\frac{1}{m} + \frac{1}{m_b}\right]^{1/2} \frac{ze}{(k_B T)^{1/2}} \frac{t_D E}{L} \frac{1}{\rho}. \qquad (1)$$

In this expression, m is the mass of the ion, m_b is the mass of a buffer gas atom, ze is the charge on the ion, ρ is the buffer gas number density, L is the length of the drift tube, E is the drift field, and t_D is the drift time. Average collision integrals obtained from the drift times are shown in Fig. 4.

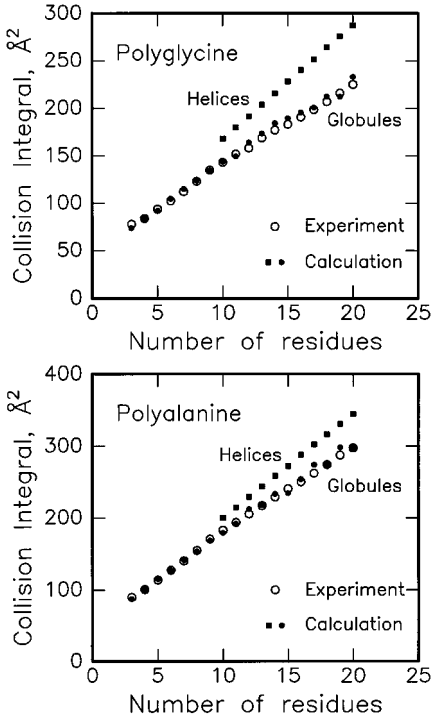

FIGURE 4 Measured and calculated collision integrals for (*A*) Gly_nH^+ and (*B*) Ala_nH^+ as a function of the number of residues at $T = 300$ K. Calculated collision integrals are shown for rigid helices and for the lowest-energy self-solvated globule conformation found in the molecular dynamics simulations.

Collision integrals calculated for rigid α-helices with all $\phi = -57^o$ and all $\psi = -47^o$ are also shown in the figure. The measured collision integrals are substantially smaller than those calculated for the helices, indicating that the larger Gly_nH^+ and Ala_nH^+ are not extended helices.

Comparison of simulations and experimental results

The conformations of Ala_n peptides have been investigated theoretically by a number of groups (Daggett and Levitt, 1992; DiCapua et al., 1991; Doruker and Bahar, 1997; Klein et al., 1996; Wang et al., 1996; Young and Brooks, 1996). Many calculations have shown than neutral Ala_n as small as Ala_{13} may form helices in vacuo (Daggett and Levitt, 1992; Wang et al., 1996). However, no simulations have previously been performed for charged Ala_nH^+ peptides of this length. The calculations that we have performed are almost certainly not sufficiently exhaustive to have located the minimum energy conformation for all of the polypeptides we have studied. For the larger peptides the most extensive simulations were performed for $Gly_{17}H^+$, $Ala_{17}H^+$, and $Ala_{19}H^+$.

The four lowest energy conformations found for $Ala_{19}H^+$ are shown in Fig. 5. The lowest energy conformation, Fig. 5 *a*, was produced by starting from an α-helix. The helix collapsed early in the simulation. In fact, α-helices for all the Ala_nH^+ peptides quickly collapsed in the simulations at 300 K. The other three conformations shown in Fig. 5 were produced by starting from different extended conformations. In all cases the peptide has balled-up to maximize intramolecular interactions with the charged N terminus.

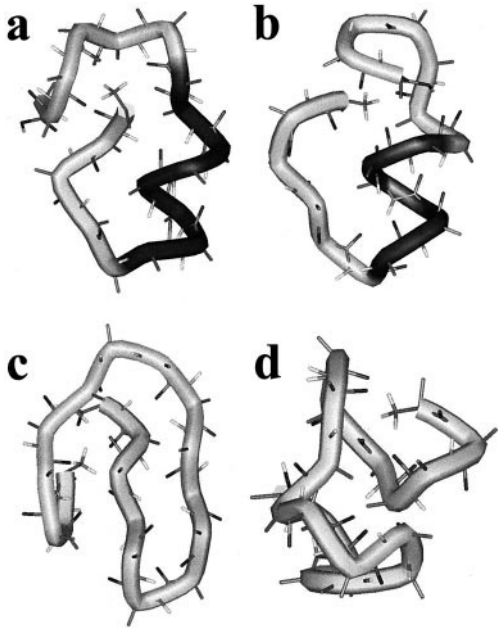

FIGURE 5 The four lowest energy conformations found in the molecular dynamics simulations for $Ala_{19}H^+$. The excess proton is located at the tetrahedral end.

We will refer to this type of conformation as a self-solvated globule. In similar simulations for neutral Ala_{19}, the helix does not unravel. This indicates that the charge disrupts the helix in vacuo.

A small helical region persists in Fig. 5 *a*, the conformation that was started from an extended helix. A small helical region is also apparent in Fig. 5 *b*, the second lowest energy conformation found in our simulations, though in this case the helical region developed during the simulation. Fig. 5 *c* has a kinked antiparallel β sheet character, whereas Fig. 5 *d* has no obvious secondary structure. Several of the low energy conformations found for $Ala_{17}H^+$ also had short helical regions, but helical regions were not observed in the simulations for $Gly_{17}H^+$. Table 1 shows the total energies and calculated collision integrals for the four low energy $Ala_{19}H^+$ conformations shown in Fig. 5. We expect the measured and calculated collision integrals to be within 2% if the conformation is correct. The ratio of the calculated and measured collision integrals for the lowest energy conformation, Fig. 5 *a*, is just outside of this range. However, the other three low energy conformations fall within the expected range.

In order to examine the interconversion between the low energy conformations we ran molecular dynamics simulations for $Ala_{17}H^+$ at elevated temperatures. Raising the temperature provides a way to rapidly search the energy landscape (Daura et al., 1997). According to these simulations, $Ala_{17}H^+$ readily interconverts between completely different conformations at 700 K, and partial rearrangements occur on the time scale of the simulations (1 ns) at 500 K. Conformations with small helical regions are present as low energy structures in the simulations at 500 and at 700 K. Distinctly different conformations persist for 50–100 ps at 700 K. This is equivalent to a rate constant of around 10^{10} s^{-1} for movement between different minima. Assuming Arrhenius behavior with an upper limit for the preexponential factor of 10^{14} s^{-1} (a molecular vibration is 10^{13}–10^{14} s^{-1}) provides an upper limit for the activation barrier for movement between different minima of approximately 54 kJ mol^{-1}. Using these parameters, the lower limit for the rate constant at 300 K is 10^4–10^5 s^{-1} and the upper limit for the lifetime is 10^{-4}–10^{-5} s^{-1}. The time scale for our measurements is substantially slower (~100 ms). Thus substantial conformational changes are expected to occur rapidly on the time scale of the mobility measurements. This should result in a relatively narrow peak at a position corresponding to the average collision integral.

We have shown in Fig. 4 the collision integrals calculated for the lowest energy conformation found in the molecular dynamics simulations for each of the polyglycine and polyalanine peptides studied. All of the conformations found were self-solvated globules. Because only one conformation is used for each species, the appropriate averaging is absent, and the predicted cross-sections do not increase smoothly with *n*. For the small polypeptides there is good agreement between the measured and calculated collision integrals. The number of different low energy conformations is relatively small for the smaller peptides. For the larger peptides, the agreement between the measured and calculated collision integrals is not as good, and the calculated collision integrals for near neighbors often show substantial fluctuations. Although we have almost certainly not identified the global minima in the simulations, the fluctuations probably result primarily from inadequate conformational averaging. The increased widths of the peaks measured for the larger peptides suggests that complete conformational averaging does not occur for these species on the time scale of the experiments because of the enormous number of conformations that are accessible.

Fig. 6 shows a plot of the total energy per residue versus the number of residues, for the lowest energy conformations found for both Gly_nH^+ and Ala_nH^+. For both systems, a minimum in the energy per residue occurs at 5–10 residues. This minimum reflects the development of the self-solvation shell around the charged terminal amine. The energy per residue becomes more negative for small peptides as the

TABLE 1 Total energies and calculated collision integrals for the four low energy conformations shown in Figure 5

Conformation	Secondary structure	Total energy, kJ mol^{-1}	Collision integral, Å^2	Calculated/ measured collision integral
Experiment	—	—	287	—
Extended helix	Helix	—	331	1.153
a	Partially helical	−2507	298	1.038
b	Partially helical	−2490	284	0.989
c	Kinked sheet	−2476	292	1.017
d	None	−2475	284	0.989

The measured collision integral and the calculated collision integral for an extended helix are also shown.

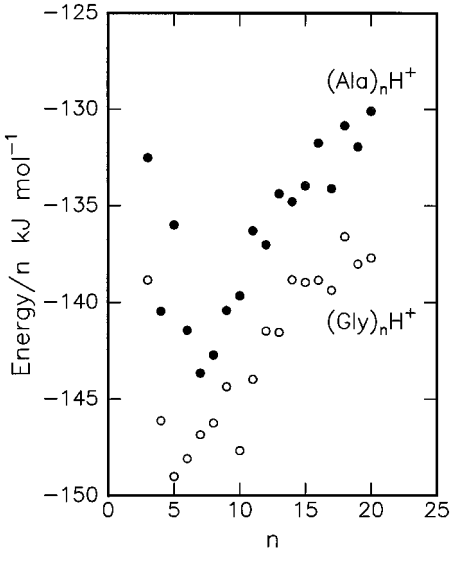

FIGURE 6 Plot of the energy per residue against the number of residues for the lowest energy conformations found for Gly_nH^+ and Ala_nH^+ in the molecular dynamics simulations.

self-solvation shell develops, but then for larger peptides crowding prevents additional residues from contributing to the solvation shell and the energy per residue becomes less negative again. The self-solvation shell is formed by hydrogen bonding interactions with backbone carbonyl groups. For the larger peptides 4–6 carbonyl groups are involved. For example, for the lowest energy conformation found for Ala_7H^+, residues 3, 5, 6, and 7 hydrogen bond to the terminal NH_3^+. As the peptide grows, there is an opportunity to form additional intramolecular hydrogen bonds not involving the terminal amine. In the simulations, the threshold for forming additional hydrogen bonds is at around $n = 9$ for both Ala_nH^+ and Gly_nH^+. For example, for Ala_9H^+ there are additional hydrogen bonds (from backbone NH to backbone CO groups) between residues 2 and 5 and between 3 and 8. These H-bonds are essentially the same as those found for the uncharged peptide.

Comparison with solution behavior

In solution, a helix-coil transition is observed for some peptides upon variation of the solution conditions. Alanine-based peptides show around 50% less helical content at 25°C than they do at 2°C (Marqusee et al., 1989). NMR studies indicate that at room temperature there is an ensemble of molecules with varying helical content, rather than just helical and nonhelical conformations. Thus, the partially helical conformations present in the molecular dynamics simulations of the protonated gas-phase peptides may be analogous to the partially helical conformations present under some solution conditions. However, globular conformations with small helical regions are indistinguishable in our studies from globular conformations without small helical regions. Thus, there is no direct experimental evidence for the presence of small helical regions in the conformations of protonated polyalanines in the gas phase. Our experimental measurements only rule out the presence of large helical regions. Although protonated polyalanines do not to form extended helices in the gas phase, there has been a report (Kaltashov and Fenselau, 1997) that melittin, a 26-residue peptide, retains its helical conformation in the gas phase, even in the $(M + 3H)^{3+}$ charge state. So apparently the charge does not always destabilize helices in the gas phase. More studies are required to identify the factors responsible for helix stability in vacuum.

CONCLUSIONS

The measured collision integrals of Gly_nH^+ and Ala_nH^+, $n = 3$–20, peptides indicate a self-solvated globule conformation, in which the peptide chain wraps around and self-solvates the charge. In molecular dynamics simulations, the charge destabilizes helical conformations, and extended helices, which persist for long times in simulations for neutral Ala_n peptides, quickly collapse (at 300 K) to self-solvated globules. An analysis of simulations performed at elevated temperatures suggests that there is an ensemble of conformations that interconvert rapidly on the time scale of the experiments. Small helical regions were observed in the simulations for protonated polyalanine peptides, but not for protonated polyglycines. Ala_nH^+ peptides with small helical regions may be related to partially helical conformations observed under some solution conditions; however, the presence of these small helical regions could not be directly confirmed by the experimental measurements.

We thank Prof. Annelise Barron and her group for the use of their peptide synthesizer and for their help in using it. MFJ acknowledges the National Science Foundation and the donors of the Petroleum Research Fund, administered by the American Chemical Society, for partial support of this study. MAR acknowledges the National Science Foundation and the DOE/LBL Advanced Batteries Program for support. We are also grateful to Jason M. Tenenbaum for help with some of the studies.

REFERENCES

Brooks, B. R., R. E. Bruccoleri, B. D. Olafson, D. J. States, S. Swaminathan, and M. Karplus. 1983. CHARMM: a program for macromolecular energy minimization and dynamics calculations. *J. Comput. Chem.* 4:187–217.

Chakrabartty, A. and R. L. Baldwin. 1995. Stability of α-helices. *Adv. Protein Chem.* 46:141–176.

Chou, P. Y. and G. D. Fasman. 1974. Prediction of protein conformation. *Biochemistry.* 13:222–245.

Clemmer, D. E., R. R. Hudgins, and M. F. Jarrold. 1995. Naked protein conformations: cytochrome *c* in the gas phase. *J. Am. Chem. Soc.* 117:10141–10142.

Collings, B. A., and D. J. Douglas. 1996. Conformation of gas-phase myoglobin ions. *J. Am. Chem. Soc.* 118:4488–4489.

Counterman, A. E., S. J. Valentine, C. A. Srebalus, S.C. Henderson, C. S. Hoagland, D. E. Clemmer. 1998. High-order structure and dissociation of gaseous peptide aggregates that are hidden in mass spectra. *J. Am. Soc. Mass. Spectrom.* 9:743–759.

Daggett, V., and M. Levitt. 1992. Molecular dynamics simulations of helix denaturation. *J. Mol. Biol.* 223:1121–1138.

Daura, X., W. van Gunsteren, D. Rigo, B. Jaun, and D. Seebach. 1997. Studying the stability of a helical β-heptapeptide by molecular dynamics simulations. *Chem. Eur. J.* 3:1410–1417.

DiCapua, F. M., S. Swaminathan, and D. L. Beveridge. 1991. Theoretical evidence for water insertion in α-helix bending: molecular dynamics of Gly_{30} and Ala_{30} in vacuo and in solution. *J. Am. Chem. Soc.* 113: 6145–6155.

Doruker, P., and I. Bahar. 1997. Role of water on unfolding kinetics of helical peptides studied by molecular dynamics simulations. *Biophys. J.* 72:2445–2456.

Dugourd, P., R. R. Hudgins, D. E. Clemmer, and M. F. Jarrold. 1997. High-resolution ion mobility measurements. *Rev. Sci. Instrum.* 68: 1122–1129.

Gross, D. S., P. D. Schnier, S. E. Rodriguez-Cruz, C. K. Fagerquist, and E. R. Williams. 1996. Conformations and folding of lysozyme ions in vacuo. *Proc. Natl. Acad. Sci. USA.* 93:3143–3148.

Hudgins, R. R., J. Woenckhaus, and M. F. Jarrold. 1997. High resolution ion mobility measurements for gas phase proteins: correlation between solution phase and gas phase conformations. *Int. J. Mass. Spectrom. Ion. Proc.* 165/166:497–507.

Kaltashov, I. A., and C. Fenselau. 1997. Stability of secondary structural elements in a solvent-free environment: the α-helix. *Proteins Struct. Funct. Genet.* 27:165–170.

Klassen, J. S., A. T. Blades, and P. Kebarle. 1995. Determinations of ion-molecule equilibria involving ions produced by electrospray: hydration of protonated amines, diamines, and some small peptides. *J. Phys. Chem.* 99:15509–15517.

Klein, C. T., B. Mayer, G. Kohler, and P. Wolschann. 1996. Influence of solvation on helix formation of poly-alanine studied by multiple annealing simulations. *J. Mol. Struct.* 370:33–43.

Marqusee, S., V. H. Robbins, and R. L. Baldwin. 1989. Unusually stable helix formation in short alanine-based peptides. *Proc. Natl. Acad. Sci. USA* 86:5286–5290.

Mason, E. A., and E. W. McDaniel. 1988. Transport Properties of Ions in Gases. Wiley-Liss, Inc., New York.

Mesleh, M. F., J. M. Hunter, A. A. Shvartsburg, G. C. Schatz, and M. E. Jarrold. 1996. Structural information from ion mobility measurements: effects of the long-range potential. *J. Phys. Chem.* 100:16082–16086.

O'Neil, K. T., and W. F. DeGrado. 1990. A thermodynamic scale for the helix-forming tendencies of the commonly occurring amino acids. *Science.* 250:646–651.

Suckau, D., Y. Shi, S. C. Beu, M. W. Senko, J. P. Quinn, F. M. Wampler, and F. W. McLafferty. 1993. Coexisting stable conformations of gaseous protein ions. *Proc. Natl. Acad. Sci. USA.* 90:790–793.

Sullivan, P. A., J. Axelsson, S. Altmann, A. P. Quist, B. U. R. Sundqvist, and C. T. Reimann. 1996. Defect formation on surfaces bombarded by energetic multiply charged proteins: implications for the conformation of gas-phase electrosprayed ions. *J. Am. Soc. Mass. Spectrom.* 7:329–341.

Valentine, S. J., J. G. Anderson, A. D. Ellington, and D. E. Clemmer. 1997. Disulfide-intact and -reduced lysozyme in the gas phase: conformations and pathways of folding and unfolding. *J. Phys. Chem. B.* 101: 3891–3900.

Van Gunsteren, W. F., and H. J. Berendsen. 1977. Algorithms for macromolecular dynamics and constraint dynamics. *Mol. Phys.* 34:1311–1327.

Wang, L., T. O'Connell, A. Tropsha, and J. Hermans. 1996. Energetic decomposition of the α-helix-coil equilibrium of a dynamic model system. *Biopolymers.* 39:479–489.

Weiner, S. J., P. A. Kollman, D. A. Case, U. C. Singh, C. Ghio, G. Alagona, S. Profeta, and P. Weiner. 1984. A new force field for molecular mechanical simulation of nucleic acids and proteins. *J. Am. Chem. Soc.* 106:765–784.

Wyttenbach, T., J. E. Bushnell, M. T. Bowers. 1998. Salt bridge structures in the absence of solvent: the case for the oligoglycines. *J. Am. Chem. Soc.* 120:5098–5103.

Wyttenbach, T., G. von Helden, and M. T. Bowers. 1996. Gas-phase conformation of biological molecules: bradykinin. *J. Am. Chem. Soc.* 118:8355–8364.

Young, W. S., and C. L. Brooks. 1996. A microscopic view of helix propagation: N and C-terminal helix growth in alanine helices. *J. Mol. Biol.* 259:560–572.

Zhang, K., D. M. Zimmerman, A. Chung-Phillips, and C. J. Cassady. 1993. Experimental and ab initio studies of the gas-phase basicities of polyglycines. *J. Am. Chem. Soc.* 115:10812–10822.